Acta Crystallographica Section A
Foundations of Crystallography
ISSN 0108-7673

Received 8 August 2000
Accepted 20 February 2001

Phase determination and extension using X-ray multiple diffraction and the maximum-entropy method

Chien-Mei Wang,[a] Chun-Hsiung Chao[a,b] and Shih-Lin Chang[a,b]*

[a]Department of Physics, National Tsing Hua University, Hsinchu, Taiwan, and [b]Synchrotron Radiation Research Center, Hsinchu, Taiwan. Correspondence e-mail: slchang@phys.nthu.edu.tw

The extension of the phases of the structure factors of the organic crystal $C_{25}H_{25}NO_2$ from 77 starting individual phases using the maximum-entropy method is reported. These starting phases were determined from 90 experimental triplet phases calculated from 215 measured ψ-scan three-beam and four-beam diffraction profiles obtained with a rotating-anode X-ray source, where the ψ scans were around the reciprocal-lattice vectors of the 001, 002 and 003 reflections. The extension of the structure factors with phase values was carried out using the maximum-entropy method for 2040 measured two-beam Bragg diffraction intensities with 77 starting phases and the symmetry of the space group as the constraints. Use of structure-factor triplets as constraints for entropy maximization was also attempted. The minimum χ^2 criteria were applied to the maximum-entropy extrapolation to discern the best phase set to be used as the new constraints for the next step of generating new phases. With this phase-extension procedure, more than 100 phases were determined and an electron-density map at 1.97 Å was deduced.

1. Introduction

Intensity measurements often provide no phase information in physics experiments. This is also true for X-ray diffraction from crystals because the intensity of a Bragg reflection is proportional to the product of the associated structure factor and its complex conjugate. The phase information of the structure factor is therefore lost. This fact constitutes the well known X-ray phase problem in diffraction physics and X-ray crystallography. In the literature, there are several ways of solving this problem, such as the direct-method heavy-atom method (see, for example, Schenk, 1991), maximum-entropy methods (see, for example, Bricogne, 1984) and many others (see, for example, Rossmann, 1972; Woolfson & Fan, 1995). On the other hand, multiple diffraction techniques, utilizing the coherent interaction among diffracted beams to extract phase information from intensity measurements, have recently demonstrated their capability of direct phase determination. This includes the qualitative determination (Post, 1977; Chapman *et al.*, 1981; Chang, 1982; Juretschke, 1982; Hümmer & Billy, 1982; Høier & Marthinsen, 1983; Mo *et al.*, 1988; Shen, 1998; and many others cited in Weckert & Hümmer, 1997 and Chang, 1998), semiquantitative determination (Shen & Colella, 1987; Hümmer *et al.*, 1989) and quantitative determination (Chang & Tang, 1988; Hümmer *et al.*, 1990; Chang, Stetsko *et al.*, 1999) of the phases of structure-factor multiplets of small (Hümmer *et al.*, 1989; Chang & Tang, 1988; Shen & Finkelstein, 1990) and macromolecular crystals (Hümmer, Schwegle & Weckert, 1991; Chang *et al.*, 1991; Weckert *et al.*, 1993; Huang *et al.*, 1994; Mo *et al.*, 1998; Chang, Chao *et al.*, 1999; Weckert *et al.*, 1999; Hölzer *et al.*, 2000; Shen *et al.*, 2000). Although this potentially useful technique gives a direct measure of phases, we are still facing challenging problems in how to make this physical phasing technique practical. For example, to determine in a short time a large number of useful reflection phases or even electron-density maps is one of the urgent issues, especially for crystals involving a large number of independent atoms in an asymmetric crystal unit cell. The conventional Renninger scan (Renninger, 1937) and the recently developed reference-beam (Shen, 1998) and stereoscopic multibeam imaging techniques (Chang, Chao *et al.*, 1999) can only provide multibeam intensity profiles for relatively strong reflections. For multiple diffraction involving weak reflections, useful three-beam profiles may not always be retainable. In addition, for the analysis of crystal structure, the phase information for as many reflections as possible is required. Moreover, the fact that some macromolecular crystals may deteriorate during the exposure to X-radiation at room temperature imposes the need for phase extension from the limited number of experimentally accessible phases to those reflections of unknown phases. In this paper, we present the details of the approach for phase extension and refinement by combining the multiple diffraction technique with the maximum-entropy principles (Chang & Wang, 1996). Namely, we first use this diffraction method to have a number of phases determined and phase relationships among reflections estab-

lished and then, with these known phases and phase relations as the constraints, employ the maximum-entropy method to infer new phases. As a step to test the validity of this approach, we used an organic crystal of known structure as a case study.

2. Experimental

In a multiple diffraction experiment, usually the crystal is first aligned for a (primary) reflection, say G, and is then rotated around the reciprocal-lattice vector **g** of this G reflection, say ψ scan. This rotation could bring an additional set of planes of the secondary reflection L into position to diffract the incident beam (see, for example, Chang, 1984). The interaction among the diffracted beams within the crystal gives rise to intensity variation on the primary reflection I_G. The multiple diffraction pattern, I_G *versus* ψ, of this three-beam interaction $(G/L/G-L)$ is thus obtained, where $G-L$ is the coupling between the primary reflection G and the secondary reflection L. The phase δ_3 of the structure-factor triplet $F_L F_{G-L}/F_G$ can be quantitatively determined (Chang & Tang, 1988; Chang *et al.*, 1991) by analyzing the intensity profiles of a single three-beam or two centrosymmetrically related three-beam diffractions (Hümmer *et al.*, 1990). More specifically, $\cos\delta_3$ depends on the intensities at the half-maxima (or minima) and $\sin\delta_3$ is proportional to the intensities at the maximum (or minimum). For four-beam diffractions $(G/L1, L2/G-L1, G-L2)$ involving a rotation of a twofold or a twofold screw axis (Hümmer, Bondza & Weckert, 1991), this criterion in phase determination still holds, where $L1$ and $L2$ are the two secondary reflections. The predominant δ_3 is therefore the phase of $F_{L1}F_{G-L1}/F_G$. The triplet phase values are usually determined with an accuracy of about 20 to 40° for relatively strong multiple diffraction (Chang *et al.*, 1991). For very weak diffraction, the error in the determined phase could be large. To determine the phase δ of each individual structure factor F, a number of triplet phases with the involved reflections G, L and $G-L$ linked with the space-group symmetry are required (Han & Chang, 1983).

Experimentally, we chose the organic crystal (3*R*,5*S*,6*R*)-3-benzyl-4, 5-dimethyl-3, 6-diphenylperhydro-1, 4-oxazin-2-one, $C_{25}H_{25}NO_2$ [space group $P2_12_12$, cell dimensions: $a = 20.2992$, $b = 14.8558$, $c = 6.9830$ Å, 4 molecules in a unit cell (Chang *et al.*, 1994)] as a test sample for illustration. The multiple diffraction experiments were performed with an 18 kW rotating-anode X-ray source. The angular divergences of X-rays from a Cu anode incident on the sample were trimmed down to 0.03° in both the vertical and horizontal directions by using two sets of slits, at the front and the exit ends of a 37 cm long evacuated beam pipe. The crystal was mounted on a modified $4+1$-circle Huber diffractometer where the fifth circle was for the detector motion in the vertical plane to monitor the secondary reflection. A scintillation counter with a receiving slit 0.5×0.5 mm in front of it was used as the detector. Cu $K\alpha_1$ radiation (wavelength $\lambda = 1.54056$ Å) was employed. The distances from the source to the crystal and from the crystal to the first collimating slit placed before the crystal were 82 and 10 cm, respectively. The distance from the crystal to the receiving slit was 39 cm. The 001, 00$\bar{1}$, 002, 00$\bar{2}$, 003 and 00$\bar{3}$ were chosen as the primary reflections for various ψ scans. The reason for choosing low-index reflections along basis vectors is to increase the link among the structure-factor triplets. 215 ψ-scan profiles were obtained. For illustration, Figs. 1 and 2 are the four-beam diffraction profiles, $I(003)$ and $I(00\bar{3})$ *versus* ψ, for $(00\bar{3})/(10\bar{1})(10\bar{2})/(\bar{1}0\bar{2})(\bar{1}0\bar{1})$ and $(003)/(\bar{2}\bar{5}1)(\bar{2}\bar{5}2)/(252)(251)$ cases, respectively. IN and OUT indicate the diffraction occurs as the reciprocal-lattice point of the secondary reflection moves towards (incoming) and leaves from (outgoing) the surface of the Ewald sphere.

3. Experimental determination of the starting phase set

The corresponding triplet phase values to the measured three-beam and four-beam diffraction profiles were determined according to the quantitative analysis procedure reported by Chang & Tang (1988) and Chang *et al.* (1991): For a given three-beam diffraction, $(0, G, L)$, the relative intensity distribution I_G of the primary reflection G is considered as the sum of the phase-dependent (dynamical) part I_D and the phase-independent (kinematical) part I_K:

$$I_G(\Delta\psi) = [I_G(3) - I_G(2)]/I_G(2) = I_D + I_K, \qquad (1)$$

where $I_G(2)$ and $I_G(3)$ are the two- and three-beam intensities of the primary reflection, respectively. And $\Delta\psi = \psi - \psi_0$, ψ_0 being the angular position at the exact three-beam point. According to Chang & Tang (1988), I_K is a symmetric function of $(\Delta\psi)$, *i.e.*

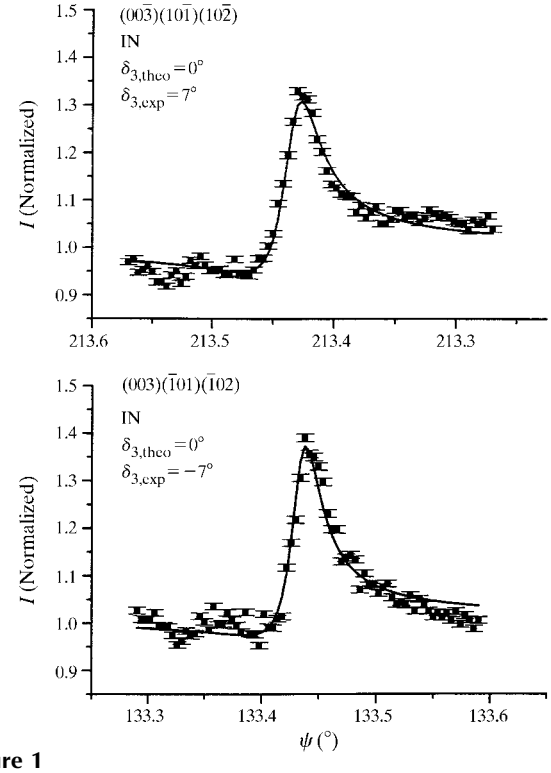

Figure 1
Multiple-diffraction profiles of four-beam cases: (000)(00$\bar{3}$)(10$\bar{1}$)(10$\bar{2}$) and (000)(003)($\bar{1}$01)($\bar{1}$02). The theoretical and experimental phase values are indicated.

$$I_K = A(\eta/2)^2 L(\Delta\psi) \tag{2}$$

and I_D can be expressed as

$$I_D = B[2(\Delta\psi)\cos\delta_3 - \eta\sin\delta_3]L(\Delta\psi), \tag{3}$$

where the proportionality constants A and B are related to the structure-factor product $|F_{G-L}||F_L|/|F_G|$ and Lorentz–polarization factor, and $L(\Delta\psi)$ is defined as

$$L(\Delta\psi) = 1/[(\Delta\psi)^2 + (\eta/2)^2]. \tag{4}$$

η is the FWHM of the three-beam diffraction profile. In principle, the quantities A, B, δ_3, ψ_0 and even η could be determined by least-squares fitting of the diffraction profile with the calculated one from (1). In practice, for more reliable phase determination, the two centrosymmetrically related three-beam diffractions, say case $A = (0, G, L)$ and case $B = (0, -G, -L)$, provide the following relationship:

$$B[2\Delta(\psi)\cos\delta + \eta\sin\delta]L = I_{GA}(\Delta\psi) - A(\eta/2)L \tag{5}$$

and the term A satisfies

$$I_{GA}(\Delta\psi = 0) + I_{GB}(\Delta\psi = 0) = 2A. \tag{6}$$

Again, with least-squares fitting, the parameters B, ψ_0, η and δ can be optimized for (5). For convenience, ψ_0 and η were determined experimentally. Thus the phase δ was determined accordingly. Similarly, predominant triplet phases associated with four-beam diffractions, involving a 2 or 2_1 rotation axis, can also be determined. An alternative is to employ the quasi-universal function and to determine the phases from the intensity ratios at maximum and minimum (Chang, Stetsko *et al.*, 1999).

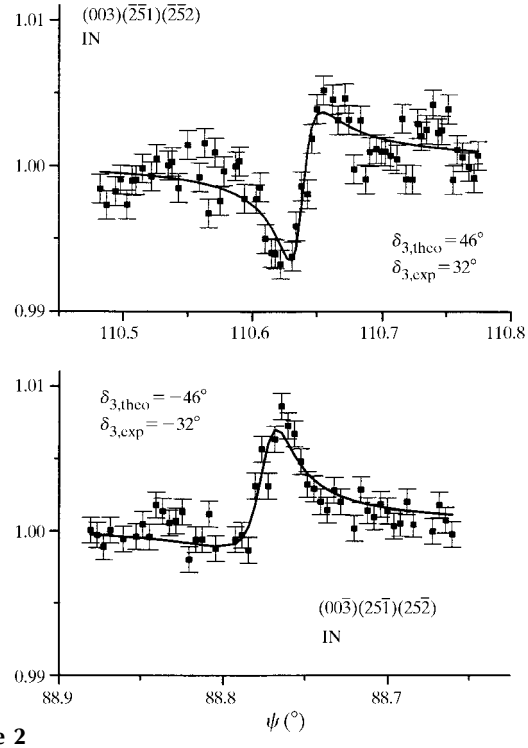

Figure 2
Multiple diffraction profiles of four-beam cases: (000)(003)($\bar{2}\bar{5}1$)($\bar{2}\bar{5}2$) and (000)(00$\bar{3}$)(25$\bar{1}$)(25$\bar{2}$).

Using this procedure, 90 triplet phases (sums) were determined from 215 ψ-scan profiles. From these triplet phase sums, the phases of 77 individual reflections were determined, which are listed in Table 1. Among these determined phases, five have errors larger than 40° owing to the involvement of weak multiple diffraction. To illustrate the phase-determination procedure, we show below the steps towards the determination of the (002) phase: From the four-beam cases, (00$\bar{1}$)/(23$\bar{1}$)(230)/($\bar{2}\bar{3}$0)($\bar{2}\bar{3}\bar{1}$), (00$\bar{3}$)/(230)(23$\bar{3}$)/($\bar{2}\bar{3}\bar{3}$)($\bar{2}\bar{3}$0), (00$\bar{1}$)/(231)(23$\bar{2}$)/($\bar{2}\bar{3}\bar{2}$)($\bar{2}\bar{3}\bar{1}$), (00$\bar{3}$)/(23$\bar{1}$)(23$\bar{2}$)/($\bar{2}\bar{3}\bar{2}$)($\bar{2}\bar{3}\bar{1}$), (00$\bar{2}$)/(231)(23$\bar{3}$)/($\bar{2}\bar{3}\bar{3}$)($\bar{2}\bar{3}\bar{1}$) and the three-beam case, (00$\bar{2}$)/(23$\bar{1}$)/($\bar{2}\bar{3}\bar{1}$), the following phase sums are obtained according to Table 2:

$$-\delta(00\bar{1}) + \delta(23\bar{1}) + \delta(\bar{2}\bar{3}0) = 178^\circ$$
$$-\delta(00\bar{3}) + \delta(230) + \delta(\bar{2}\bar{3}\bar{3}) = 354^\circ$$
$$\Rightarrow \delta(001) + \delta(003) - \delta(231) - \delta(233) = 532^\circ \tag{7}$$
$$-\delta(00\bar{1}) + \delta(231) + \delta(\bar{2}\bar{3}\bar{2}) = 185^\circ$$
$$-\delta(00\bar{3}) + \delta(23\bar{1}) + \delta(\bar{2}\bar{3}\bar{2}) = 173^\circ$$
$$\Rightarrow \delta(001) + \delta(003) + 2\delta(231) = 12^\circ \tag{8}$$
$$-\delta(00\bar{2}) + \delta(23\bar{1}) + \delta(\bar{2}\bar{3}\bar{1}) = 341^\circ$$
$$\Rightarrow \delta(231) = \tfrac{1}{2}\delta(002) - 171^\circ \tag{9}$$
$$-\delta(00\bar{2}) + \delta(231) + \delta(\bar{2}\bar{3}\bar{3}) = 236^\circ$$
$$\Rightarrow \delta(233) = \tfrac{3}{2}\delta(002) - 407^\circ \tag{10}$$
$$\delta(001) - 2\delta(002) + \delta(003) = 315^\circ \tag{11}$$
$$\delta(001) + \delta(002) + \delta(003) = 353^\circ. \tag{12}$$

The phase relations due to the symmetry of the space group $P2_12_12$ are employed. Equations (11) and (12) are obtained from the sum of (7) + (9) + (10) and the combination of (8) and (9), respectively. This leads to

$$\delta(002) = 13^\circ. \tag{13}$$

According to the space group, we set $\delta(002) = 0^\circ$ for the centric 002 reflection. Similar procedures are carried out for the other triplet phase sums that lead to 77 determined individual phases, among which 30 are centric and 47 are acentric reflections.

4. Phase extension using maximization of entropy

The procedure of phase extension, based on the principle of entropy maximization, starts with the experimentally determined phases and amplitudes of the structure factors and the structure-factor triplets as the constraints. The entropy S of the electron distribution in the crystal unit cell is written as

$$S = -\sum_{\mathbf{r}} \rho(\mathbf{r})\ln[\rho(\mathbf{r})/m(\mathbf{r})], \tag{14}$$

where the electron density $\rho(\mathbf{r})$ is considered as the probability of finding an electron at the position $\mathbf{r}$, and $m(\mathbf{r})$ is the uniformly distributed electron density (*i.e.* no prior map is used). To maximize the entropy, the Lagrangian multiplier technique is used where the Lagrangian L takes the form

$$L = S + \sum_H [\lambda_{Hr} C_{Hr} + \lambda_{Hi} C_{Hi}] + \sum_{KL} [\lambda_{KLr} C_{KLr} + \lambda_{KLi} C_{KLi}], \quad (15)$$

where C_{Hr} and C_{Hi} are the constraints on the real and the imaginary parts of the difference between the calculated F_H^c from entropy maximization and the experimental F_H^0 determined from two-beam Bragg reflection and multiple diffraction intensity. C_{KLr} and C_{KLi} are the constraints on the real and the imaginary parts of the differences between the calculated and the measured triplets $F_H F_K F_L$. The λ's are the Lagrangian multipliers.

Since there are differences in magnitude between F_H and the triplets $F_H F_K F_L$, we first calculate λ_{Hr} and λ_{Hi} of (15) by treating the C_{Hr} and C_{Hi} as the zeroth-order perturbation and then look for λ_{KLr} and λ_{KLi} using the C_{KLr} and C_{KLi} as the first-order perturbation. Because F_H can be first optimized in the zeroth-order calculation, the subsequent optimization of $F_H F_K F_L$ can be simplified by considering only the product $F_K F_L$. The constraints C can be expressed as

$$C_{Hr} = F_H^c - |F_H^0| \cos \delta_H^0 \quad (16a)$$

$$C_{Hi} = F_{Hi}^c - |F_H^0| \sin \delta_H^0 \quad (16b)$$

$$C_{KLr} = F_{Kr}^c F_{Lr}^c - F_{Ki}^c F_{Li}^c - F_K^0 F_L^0 \cos(\delta_K + \delta_L) \quad (16c)$$

$$C_{KLi} = F_{Lr}^c F_{Ki}^c - F_{Kr}^c F_{Li}^c - F_K^0 F_L^0 \sin(\delta_H + \delta_L), \quad (16d)$$

where the phase sum $\delta_K + \delta_L = \delta_3^0(HKL) - \delta_H^0$, δ_H being the phase of F_H and $\delta_3(HKL)$ the triplet phase of $F_H F_K F_L$. The superscripts c and 0 stand for the calculated and the observed values, respectively. Following the maximization procedure, *i.e.* $\partial L/\partial \rho = 0$, the zeroth-order and the first-order electron densities take the forms:

$$\rho_0(\mathbf{r}) = m(\mathbf{r}) \exp\left\{-1 + \sum_H [\lambda_{Hr} \cos 2\pi \mathbf{H}\cdot\mathbf{r} + \lambda_{Hi} \sin 2\pi \mathbf{H}\cdot\mathbf{r}]\right\} \quad (17)$$

$$\begin{aligned}\rho_1(\mathbf{r}) = \rho_0(\mathbf{r}) \exp\Big\{ &\sum_{K,L} [(\lambda_{KLr} F_{Kr}^c + \lambda_{KLi} F_{Ki}^c) \cos 2\pi \mathbf{L}\cdot\mathbf{r} \\ &+ (\lambda_{KLi} F_{Kr}^c + \lambda_{KLr} F_{Ki}^c) \sin 2\pi \mathbf{L}\cdot\mathbf{r} \\ &+ (\lambda_{KLr} F_{Lr}^c + \lambda_{KLi} F_{Li}^c) \cos 2\pi \mathbf{K}\cdot\mathbf{r} \\ &+ (\lambda_{KLi} F_{Lr}^c + \lambda_{KLr} F_{Li}^c) \sin 2\pi \mathbf{K}\cdot\mathbf{r}]\Big\}, \end{aligned} \quad (18)$$

where the F^c's are calculated from ρ_0. In addition, the symmetry of the space group to which the crystal belongs is considered: Hereafter, we refer to those reflections of providing constraints as in the $\{H\}$ basis set for clarity. The numbers n_1 and n_2 are the number of the constraints involving the reflections with $h + k = 2n$ and the number of the constraints of the reflections with $h + k = 2n + 1$. By considering these two sets of reflections, the electron density $\rho(\mathbf{r})$ derived from (17) becomes

$$\rho(\mathbf{r}) = m(\mathbf{r}) \exp\left\{-1 + 2 \sum_{\substack{j=1 \\ h+k=2n}}^{n_1} w_{E_j}(\mathbf{r}) + 2 \sum_{\substack{l=1 \\ h+k=2n+1}}^{n_2} w_{O_l}(\mathbf{r})\right\}, \quad (19)$$

Table 1
The 77 individual phases derived from multiple-diffraction experiments.

No.	*hkl*	δ (°)	$\delta_{\rm th}$ (°)	No.	*hkl*	δ (°)	$\delta_{\rm th}$ (°)
1	001	180	180	2	002	0	0
3	003	180	180	4	011	90	90
5	012	−90	−90	6	013	90	90
7	031	−90	−90	8	032	−90	−90
9	033	−90	−90	10	040	180	180
11	041	0	0	12	042	180	180
13	101	−90	−90	14	102	−90	−90
15	110	180	180	16	111	67	42
17	112	51	91	18	113	108	89
19	120	0	0	20	121	−1	−6
21	122	−140	−85	22	123	111	37
23	130	180	180	24	131	−81	−66
25	132	−143	−156	26	140	0	0
27	141	154	−118	28	150	180	180
29	151	−161	−144	30	152	−55	−64
31	200	180	180	32	201	180	180
33	210	180	180	34	211	−1	−64
35	212	−167	−163	36	213	175	169
37	230	0	0	38	231	10	15
39	232	−3	−1	40	233	134	170
41	240	0	0	42	241	−77	−125
43	242	73	139	44	301	0	0
45	302	90	90	46	310	0	0
47	311	−159	−146	48	312	−34	−42
49	320	180	180	50	321	−1	−8
51	322	154	154	52	330	180	180
53	331	−82	−90	54	332	−125	−126
55	400	180	180	56	401	0	0
57	402	0	0	58	403	0	0
59	410	0	0	60	411	−82	−65
61	430	0	0	62	431	99	93
63	432	52	87	64	440	180	180
65	441	−85	−39	66	442	140	98
67	443	−165	−111	68	501	90	90
69	502	−90	−90	70	600	180	180
71	601	180	180	72	610	180	180
73	611	−72	−58	74	612	176	151
75	620	180	180	76	621	−22	−8
77	622	28	−33				

where

$$\begin{aligned} w_{E_j}(\mathbf{r}) = \lambda_{A\mathbf{H}_j} \{&\cos 2\pi[(hkl)_j \cdot \mathbf{r}] + \cos 2\pi[(\bar{h}kl)_j \cdot \mathbf{r}] \\ &+ \cos 2\pi[(h\bar{k}l)_j \cdot \mathbf{r}] + \cos 2\pi[(hk\bar{l})_j \cdot \mathbf{r}]\} \\ &+ \lambda_{B\mathbf{H}_j} \{\sin 2\pi[(hkl)_j \cdot \mathbf{r}] - \sin 2\pi[(\bar{h}kl)_j \cdot \mathbf{r}] \\ &- \sin 2\pi[(h\bar{k}l)_j \cdot \mathbf{r}] - \sin 2\pi[(hk\bar{l})_j \cdot \mathbf{r}]\} \end{aligned} \quad (20a)$$

$$\begin{aligned} w_{O_l}(\mathbf{r}) = \lambda_{A\mathbf{H}_l} \{&\cos 2\pi[(hkl)_l \cdot \mathbf{r}] - \cos 2\pi[(\bar{h}kl)_l \cdot \mathbf{r}] \\ &- \cos 2\pi[(h\bar{k}l)_l \cdot \mathbf{r}] + \cos 2\pi[(hk\bar{l})_l \cdot \mathbf{r}]\} \\ &+ \lambda_{B\mathbf{H}_l} \{\sin 2\pi[(hkl)_l \cdot \mathbf{r}] + \sin 2\pi[(\bar{h}kl)_l \cdot \mathbf{r}] \\ &+ \sin 2\pi[(h\bar{k}l)_l \cdot \mathbf{r}] - \sin 2\pi[(hk\bar{l})_l \cdot \mathbf{r}]\}. \end{aligned} \quad (20b)$$

The symmetry of the space group has been considered in deriving the w's of (20*a*) and (20*b*), and the λ's are the same for the reflections belonging to the same family $\{\mathbf{H}_j\} = \{hkl\}$. In the matrix calculation, we employ also the diagonalization technique to scale down the dimension from n^3 to n so as to speed up the calculation (Bricogne & Gilmore, 1990; Drabold & Sankey, 1993). The electron-density distribution $\rho(\mathbf{r})$ given in (19) can be calculated by the following recurrent procedures:

Table 2
The determined triplet phase invariants from the multiple diffraction experiments $\delta_3 = \delta_{(-G)} + \delta_{(L)} + \delta_{(G-L)}$ for three-beam cases $(0, G, L)$ and $\delta_3 = \delta_{(-G)} + \delta_{(L1)} + \delta_{(G-L1)} = \delta_{(-G)} + \delta_{(L2)} + \delta_{(G-L2)}$ for four-beam $(0, G, L1, L2)$ cases.

Number	Secondary reflections L	δ_3 (°) exp	δ_3 (°) theo
(i) Primary reflection $G = 00\bar{1}$			
1	$\bar{1}11, \bar{1}1\bar{2}$	163±23	−131
2	$\bar{2}10, \bar{2}1\bar{1}$	−8±19	−1
3	$031, 03\bar{2}$	167±32	180
4	$040, 04\bar{1}$	−9±23	0
5	$150, 15\bar{1}$	122±20	144
6	$140, 14\bar{1}$	26±19	298
7	$130, 13\bar{1}$	40±3	66
8	$240, 24\bar{1}$	−32±5	−55
9	$231, 23\bar{2}$	185±11	−163
10	$120, 12\bar{1}$	181±33	−173
11	$340, 34\bar{1}$	122±30	−137
12	$230, 23\bar{1}$	178±37	165
13	$440, 44\bar{1}$	85±4	39
14	$330, 33\bar{1}$	94±32	90
15	$220, 22\bar{1}$	238±28	252
16	$321, 32\bar{2}$	24±31	17
17	$430, 43\bar{1}$	84±8	87
18	$110, 11\bar{1}$	−30±5	−42
19	$211, 21\bar{2}$	−14±20	−18
20	$320, 32\bar{1}$	−17±21	8
21	$620, 62\bar{1}$	16±24	8
22	$310, 31\bar{1}$	−39±7	−34
23	$410, 41\bar{1}$	262±31	245
24	$610, 61\bar{1}$	18±18	58
25	$301, 30\bar{2}$	202±33	180
26	$600, 60\bar{1}$	179±21	180
27	$400, 40\bar{1}$	−5±12	0
28	$\bar{2}00, \bar{2}0\bar{1}$	200±25	180
29	$\bar{1}\bar{2}1, \bar{1}\bar{2}\bar{2}$	165±23	258
(ii) Primary reflection $G = 00\bar{2}$			
1	$14\bar{1}$	114±4	236
2	$231, 23\bar{3}$	236±36	−155
3	$350, 35\bar{2}$	84±7	117
4	$13\bar{1}$	163±30	133
5	$24\bar{1}$	154±23	−111
6	$01\bar{1}$	183±15	180
7	$441, 44\bar{3}$	80±1	72
8	$23\bar{1}$	341±44	−30
9	$12\bar{1}$	2±42	13
10	$44\bar{1}$	87±18	77
11	$33\bar{1}$	164±28	173
12	$110, 11\bar{2}$	105±9	89
13	$43\bar{1}$	162±28	173
14	$32\bar{1}$	3±24	17
15	$11\bar{1}$	−135±37	−84
16	$62\bar{1}$	45±30	16
17	$21\bar{1}$	2±39	2
18	$31\bar{1}$	−42±33	−67
19	$41\bar{1}$	83±13	130
20	$61\bar{1}$	144±40	116
21	$60\bar{1}$	−23±40	0
22	$50\bar{1}$	153±26	180
23	$40\bar{1}$	31±11	0
24	$30\bar{1}$	160±25	180
25	$20\bar{1}$	78±12	0
26	$10\bar{1}$	173±34	180
27	$1\bar{2}0, 1\bar{2}\bar{2}$	−140±29	−85
28	$011, 01\bar{3}$	11±39	0
29	$031, 03\bar{3}$	27±11	0
30	$160, 16\bar{2}$	−118±10	−120
31	$04\bar{1}$	22±30	0
32	$150, 15\bar{2}$	128±38	−116
33	$121, 12\bar{3}$	−112±21	−43
34	$020, 02\bar{2}$	13±10	0
35	$03\bar{1}$	156±27	180
36	$15\bar{1}$	−38±11	−71
(iii) Primary reflection $G = 00\bar{3}$			
1	$03\bar{1}, 03\bar{2}$	1±29	0
2	$25\bar{1}, 25\bar{2}$	−32±17	−46
3	$02\bar{1}, 02\bar{2}$	176±31	180
4	$13\bar{1}, 13\bar{2}$	44±14	42
5	$24\bar{1}, 24\bar{2}$	184±30	165
6	$230, 23\bar{3}$	354±26	10
7	$23\bar{1}, 23\bar{2}$	173±35	166
8	$44\bar{1}, 44\bar{2}$	125±8	120
9	$01\bar{1}, 01\bar{2}$	168±28	180
10	$33\bar{1}, 33\bar{2}$	27±20	36
11	$110, 11\bar{3}$	−108±23	−89
12	$43\bar{1}, 43\bar{2}$	29±37	0
13	$22\bar{1}, 22\bar{2}$	203±48	159
14	$53\bar{1}, 53\bar{2}$	150±15	163
15	$11,3,\bar{1}, 11,3,\bar{2}$	177±40	203
16	$62\bar{1}, 62\bar{2}$	174±15	−138
17	$61\bar{1}, 62\bar{2}$	98±17	84
18	$31\bar{1}, 31\bar{2}$	13±5	9
19	$400, 40\bar{3}$	−10±37	0
20	$50\bar{1}, 50\bar{2}$	178±27	180
21	$40\bar{1}, 40\bar{2}$	119±21	180
22	$2\bar{1}0, 2\bar{1}\bar{3}$	175±6	169
23	$10\bar{1}, 10\bar{2}$	7±43	0
24	$04\bar{1}, 04\bar{2}$	31±17	0
25	$15\bar{1}, 15\bar{2}$	37±3	28

Step 1: Set the initial values of the Lagrangian multipliers $\lambda^{(0)}_{AH_j} = \lambda^{(0)}_{BH_j} = 0.1$ for all j (based on the results of several trials).

Step 2: Substituting $\lambda^{(0)}_{AH_j}, \lambda^{(0)}_{BH_j}, j = 1, 2, \ldots, n_1 + n_2$, into (19), $\rho(\mathbf{r}) = \rho^{(1)}(\mathbf{r})$ is obtained, where $\rho^{(1)}(\mathbf{r})$ is the $\rho^{(i)}(\mathbf{r})$ with $i = 1$ (the first recurrent cycle of calculation).

Step 3: Calculate the total number of electrons $N^{(1)}$ in the unit cell from $\rho^{(1)}(\mathbf{r})$, *i.e.*

$$\sum_{\mathbf{r}} \rho^{(1)}(\mathbf{r}) = N^{(1)} \tag{21}$$

and normalize the electron-density distribution such that

$$\sum_{\mathbf{r}} q^{(1)}(\mathbf{r}) = F_{000} \tag{22}$$

with

$$q^{(1)}(\mathbf{r}) = \rho^{(1)}(\mathbf{r}) F_{000} / N^{(1)}, \tag{23}$$

where F_{000} is a reference structure-factor amplitude of the 000 reflection.

Step 4: Calculate $F^{(1)}_{H_j}$ for $j = 1, 2, \ldots, n_1 + n_2$ *via* the fast Fourier transform (FFT) of $q^{(1)}(\mathbf{r})$ and calculate also the χ^2_H as

$$\chi^2_H(1) = \sum_j |F^{(1)}_{H_j} - F^{\rm obs}_{H_j}|^2 / N, \tag{24}$$

where N is the total number of reflections used in the calculation. The summation is taken over the reflections that impose the constraints on the entropy maximization, *i.e.* over the $\{H\}$ set.

Step 5: Substitute the calculated $F^{(1)}_{H_j}, j = 1, 2, \ldots, n_1 + n_2$, into the constraints (16) and employ the Newton–Raphson method (Press *et al.*, 1992) to determine the necessary

adjustment $\delta\lambda$ on the λ's so that $F_{H_j}^{(1)}$ is within the experimental standard deviation of $F_{H_j}^{\rm obs}$. Namely,

$$\left[\frac{\partial\rho^{(1)}}{\partial\lambda_{H_j}}\right][\Delta\lambda_{H_j}] = [F_{H_j}^{(1)} - F_{H_j}^{\rm obs}]. \qquad (25)$$

From this we obtain a new set of Lagrangian multipliers:

$$\begin{cases} \lambda_{AH_j}^{(2)} = \lambda_{AH_j}^{(1)} + \delta\lambda_{AH_j}^{(1)}, \\ \lambda_{BH_j}^{(2)} = \lambda_{BH_j}^{(1)} + \delta\lambda_{BH_j}^{(1)}, \end{cases} \quad j = 1, 2, \ldots, n_1 + n_2.$$

Step 6: Repeat the same procedures as given in steps 2, 3, 4 and 5 for the new set of λ's.

Step 7: Compare the calculated $\chi_H^2(i+1)$ with $\chi_H^2(i)$: If $\chi_H^2(i+1) < \chi_H^2(i)$, then proceed with the iterative cycle from steps 3, 4, 5 and 6. If $\chi_H^2(i+1) > \chi_H^2(i)$, then stop the recurrent calculation.

Following the above steps, we first use the 77 experimental structure factors, both magnitudes and phases, and 8 forbidden reflections, 100, 300, 500, 700, 010, 030, 050 and 007 as the constraints. With these 85 reflections belonging to the $\{H\}$ set, we then refine the $\{F_{H_j}\}$ by following steps 4 and 5 so as to determine the most proper values for λ's such that a minimum value of χ_H^2 with $H \in \{H\}$ is reached. From these λ values, the electron density $\rho(\mathbf{r})$ is calculated by using (19). We then add a reflection K to the $\{H\}$ basis set. If K is a centric reflection, then we assume its phase value is either 0 or 180° and follow steps 1 to 7 to obtain a minimum χ_H^2 value, except that $\lambda_{AK}^{(0)} = 0.1$ and $\lambda_{BK}^{(0)} = 0.1$ for the K reflection. The phase δ_K is determined according to the minimum of the two calculated $\chi_H^2(\delta_K = 0°)$ and $\chi_H^2(\delta_K = 180°)$. Namely, if $\chi_H^2(\delta_K = 0°) < \chi_H^2(\delta_K = 180°)$, the correct phase is $\delta_K = 0°$. If K is an acentric reflection, its nominal phase δ can be calculated from the $\rho(\mathbf{r})$ just obtained. The possible values of δ_K are then assumed to be δ, $\delta + 90°$, $\delta + 180°$ and $\delta + 270°$, respectively, to cover the four quadrants in the phase space. Following steps 1–7, we calculate χ_H^2 for each of the assumed phases and choose as the correct phase the one with a minimum χ_H^2 value.

In the phase-extension procedure, we used the χ_H^2, calculated from the $\{H\}$ set, to select the correct phase values. For comparison, in addition to entropy S, the likelihood was also calculated as a criterion for the phase determination of the structure factors of the $\{K\}$ reflections.

According to Bricogne & Gilmore (1990), the following expressions were used for calculating the log likelihoods:

$$L_a = \sum_{\substack{k\in K \\ \text{acentric}}} \left\{ \log I_0\left[\left(\frac{2N_o}{\varepsilon_K}\right)|U_K|^{\rm obs}|U_K^{\rm ME}|\right] - \left(\frac{N_o}{\varepsilon_K}\right)|U_K^{\rm ME}|^2 \right\} \qquad (26)$$

for acentric reflections, and

$$L_c = \sum_{k\in K} \left\{ \log\cos ch\left[\left(\frac{N_o}{\varepsilon_K}\right)|U_K|^{\rm obs}|U_K^{\rm ME}|\right] - \left(\frac{N_o}{2\varepsilon_K}\right)|U_K^{\rm ME}|^2 \right\} \qquad (27)$$

for centric reflections, where I_0 is the zeroth-order modified Bessel function, ε_K is the statistical weight and N_o is the total number of atoms in the unit cell. $|U_K|^{\rm obs}$ and $U_K^{\rm ME}$ are the observed modulus of the unitary structure factor and of the maximum-entropy-deduced unitary factor, respectively.

Table 3
Entropy S, likelihood $\mathbf{L}$ and χ_H^2 values for the first few phase-extension steps.

Step	N	S	$\mathbf{L}$	$\chi_H^2 \times 10^{-5}$
1	85	−0.4396	2405.05	0.00079
2-1	89	−0.4665	2464.99	0.00080
2-2	89	−0.4638	2780.86	0.00125
2-3	89	−0.4733	2621.59	0.00100
2-4	89	−0.4717	2748.61	0.00145
2-5	89	−0.4225	2606.64	0.00081
2-6	89	−0.4214	2698.00	0.00187
2-7	89	−0.4826	2499.84	0.00162
2-8	89	−0.4786	2614.58	0.00207
3-1	91	−0.4665	2765.25	0.00098
3-2	91	−0.4729	2682.15	0.00142
3-3	91	−0.4646	2808.82	0.00165
3-4	91	−0.4635	2713.41	0.00203
4-1	93	−0.4700	2839.63	0.00219
4-2	93	−0.4700	2845.98	0.00368
4-3	93	−0.4687	2870.29	0.00329
4-4	93	−0.4702	2876.35	0.00456

5. Results and discussion

In the phase-extension calculation, the unit cell is divided into $16 \times 16 \times 8$ pixels along a, b and c axes. The 85 individual phases (Table 1), 90 triplet phases (Table 2) and the intensity measurements of the data collection for structure-factor moduli were used as the input for maximizing the entropy and determined the electron density by substituting the parameters w, calculated by the Newton–Raphson method, into (19). The same procedure as described in §4 was repeated for many cycles. The χ_H^2, entropy S and likelihood $\mathbf{L}$ were calculated accordingly. The total number of reflections in the $\{K\}$ set was $256 - 85 = 171$, where $256 = 8 \times 8 \times 4$ covers one quadrant of the $\{hkl\}$ in the reciprocal space.

The selection of a K reflection for phase extension follows the principles described below:

(i) Those reflections with the largest number of connections in the experimental triplets, *i.e.* experimental $\Sigma1$ and $\Sigma2$ relations, were chosen as the first K reflections for phase extension.

(ii) Those reflections with large values of the product $|F_k^{\rm obs}| \times |F_k^{\rm ME}|$ were selected.

(iii) Centric and acentric K reflections were chosen alternatively for phase extension.

(iv) K reflections with large d^* and small d^* were alternatively selected for phase calculation.

Following these guidelines, Tables 3, 4 and 5 list the first few steps of phase extension. Step 1 is the initial calculation for the starting 85 reflections. From steps 2-1 to 2-8, the centric reflections 730, 450, 340 and 341 were chosen for calculation. From the entropy maximization and the $\Sigma2$ relation from the triplet, No. 11 of Table 2(i), we have

$$-\delta(00\bar{1}) + \delta(340) + \delta(\bar{3}\bar{4}\bar{1}) = 122°.$$

Table 4
Input phase values (°) for phase extension, step 2.

	Step							
hkl	2-1	2-2	2-3	2-4	2-5	2-6	2-7	2-8
730	0	0	180	180	0	0	180	180
450	180	0	180	0	180	0	180	0
340	180	180	180	180	0	0	0	0
341	−122	−122	−122	−122	57	58	58	58

Namely,

$$\delta(341) = \delta(001) + \delta(340) - 122^\circ.$$

Since $\delta(001)$ is known from Table 1, the phase of 341 can be determined if the phase of 340 is known. Table 4 lists the assumed phase combination for phase-extension calculation. The entropy, likelihood and χ^2_H values are listed in Table 3. As can be seen from the definitions, S is an indicator of the electron-density distribution in the unit cell; **L** reflects the degree of consistency between the structure factors $|F_K^{\rm ME}|$ and $|F_K^{\rm obs}|$. χ^2_H is related to the matching between the structure factors $F_H^{\rm ME}$ and $F_H^{\rm obs}$ of the $\{H\}$ set, which is a strong phase-dependent parameter.

Since the λ for $16 \times 16 \times 8$ pixels is of low resolution, correct phases may not be associated with the maximum value of S. Similarly, for a small number of K reflections, the largest likelihood may not lead to the correct phases (Bricogne, 1984). In comparison with the theoretical phases calculated from the known crystal structure, we found that the above statement was correct and moreover the minimum χ^2_H seemed to give a clear indication of having correct phases determined. Hence, for steps 2-1 to 2-8, the correct phase values are $\delta(730) = 0^\circ$, $\delta(450) = \delta(340) = 180^\circ$, and $\delta(341) = -122^\circ$, as assigned in step 2-1.

The process was continued, putting in more K reflections for phase extension: In steps 3-1 to 3-4, we intended to determine the phases of the centric reflection 370 and acentric reflection 073. The phase of the latter is either 90 or −90° according to the space group. Table 5 lists the possible phase combinations for phase extension. In steps 4-1 to 4-4, we continued phase extension for centric reflection 560 and acentric reflection 072. All the phase combinations turned out to have larger χ^2_H values than the correct phase combination. This again ensured that the phase values with the lowest χ^2_H are the correct choice.

In the following steps, the phase extension was carried out for: (I) acentric 071, 671; (II) acentric 631; (III) centric 220, 510, 710 and acentric 221 and 222. For acentric reflections, we extended the phase of one reflection each step. The calculations then continued for the rest of reflections.

Several distinct capabilities and characteristics of the present approach are shown as follows:

(i) *Phase determination and refinement using individual reflections as the constraints.*

Fig. 3(*a*) shows the calculated phase δ for the 111 reflection *versus* the number N of individual reflections used as the constraints, where the initial phase value 67° of 111 was

Table 5
Input phase values (°) for phase extension, step 3.

	Step			
hkl	3-1	3-2	3-3	3-4
073	90	90	−90	−90
073	90	90	−90	−90

determined from the multiple diffraction experiments. The calculation conditions were $16 \times 16 \times 8$ pixels in the a, b, c axes respectively. As the number of constraints increases, the calculated phase value is refined to a value approaching the asymptotic value $\delta = 59^\circ$, which is closer to the theoretical value of 42° calculated from the known structure. Fig. 3(*b*) shows a similar effect on the phase determination of the 252 reflection, the phase of which was originally unknown. When the number of reflections was 150, we employed the present phase-extension procedure to calculate the χ^2_H values for the four possible phase values, δ_K, $\delta_K + 90^\circ$, $\delta_K + 180^\circ$ and $\delta_K + 270^\circ$, of this acentric reflection. The asymptotic value $\delta = 122^\circ$ with the smallest χ^2_H value is very close to the theoretical value 114°. Similarly, the convergence of the calculated phases of the 431 and 221 reflections is also obtained as the number of reflections (constraints) increases. The initial phase values of 431 and 221 used for phase extension are 98 and 32°. The former is deduced from the multiple diffraction experiments and the latter is calculated from entropy maximization. The final converged phase values are 94 and −55°, respectively.

(ii) *Phase refinement using triplet phase relations as the constraints.*

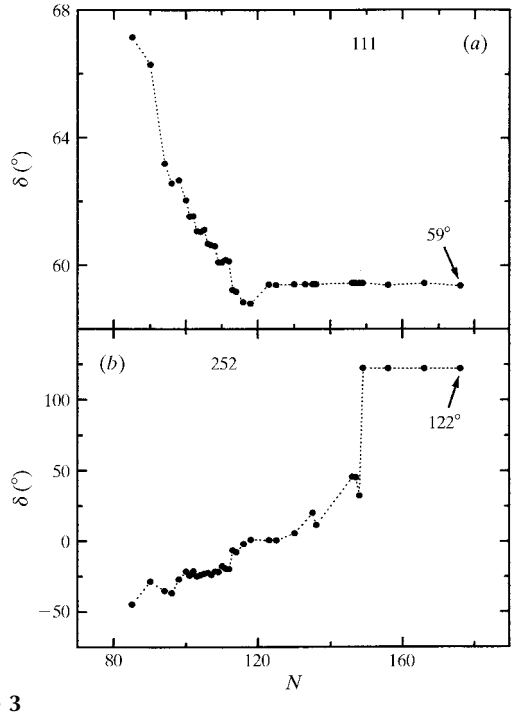

Figure 3
Convergence of the individual phase δ *versus* the number of reflections N used as the constraints for (*a*) 111 and (*b*) 252 reflections.

Following (15), the phase value of an individual reflection can be refined by using triplet relations as the constraints in entropy maximization, while maintaining the λ_{Hr} and λ_{Hi} of the individual reflections unchanged. Fig. 4 demonstrates the ability of this calculation scheme for phase refinement of the 121 and 110 reflections. The initial phase values of this figure are those calculated for maximum entropy with the individual reflections as the constraints.

(iii) *The role of* χ^2_H.

Fig. 5(*a*) shows the calculated χ^2_H values of the H set when adding each time in the H set a K reflection. Fig. 5(*b*) shows the convergence of the minimum χ^2_H as the number of iterative cycles increases for a typical situation. In Fig. 5(*a*), if the K reflection is acentric, only the maximum and minimum χ^2_H values are shown. Evidently, those correctly assigned phases have minimum χ^2_H values (solid circles). However, the corresponding overall trends of entropy S and likelihood **L** are always increasing as the number of reflections (constraints) is increased. In some phase-extension steps, especially for the small number of reflections involved, the correct phases may not necessarily be associated with the maximum values of S and **L**.

In the phase-extension procedure, the number of reflections should be comparable with the number of pixels used in order to have phases correctly determined. For $16 \times 16 \times 8$ pixels, the highest-order reflections whose phases can be correctly determined are $(\pm7, \pm7, \pm3)$. With this scheme, we are able to determine more than 100 new phases in addition to the 85 experimental phases. Also, the approximate electron-density map on the *ab* plane at 1.97 Å resolution is obtained, which is shown in Fig. 6(*a*). Comparison to the map in Fig. 6(*b*), calculated from the known structure, clearly shows fair agreement between the two maps.

6. Conclusions

The results of phase determination and extension presented in the previous section can be summarized as follows:

(i) With 85 individual reflection phases as the starting phase set, we have developed 120 additional phases *via* the maximum-entropy procedures. The average deviations in modulus and phase of the structure factor from those calculated from the known structure are about 1.5 electrons and 30°, respectively. The accuracy of the experimentally determined triplet phases from multiple diffraction patterns is on the average about 30°.

(ii) The sensitivity of χ^2_H to correct phases developed in the entropy-maximization procedure has been verified as described in §5 (see also Table 3). Moreover, a double check has been carried out by replacing F^c_H's in the constraints (16) with the calculated F_H's from the known structure. The corresponding calculated χ^2_H value becomes much smaller while the entropy and likelihood remain at almost the same values.

(iii) The choice of the pixel number, namely the spatial resolution in $\rho(\mathbf{r})$, seems affect the χ^2_H slightly at least for the present low-resolution situation. The difference in χ^2_H between $8 \times 8 \times 4$ pixels and $16 \times 16 \times 8$ pixels for 47 reflections (constraints) is less than 10%.

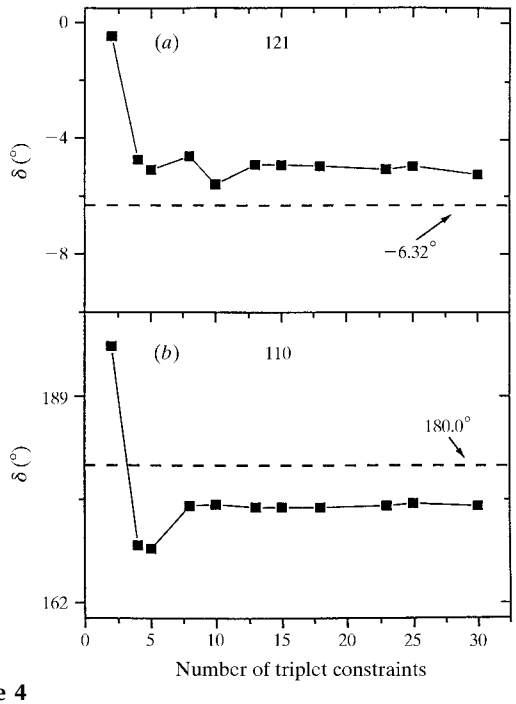

Figure 4
Convergence of the phase δ *versus* the number of triplet phase relations used as the constraints for (*a*) 121 and (*b*) 110 reflections (dashed lines: theoretical phase values).

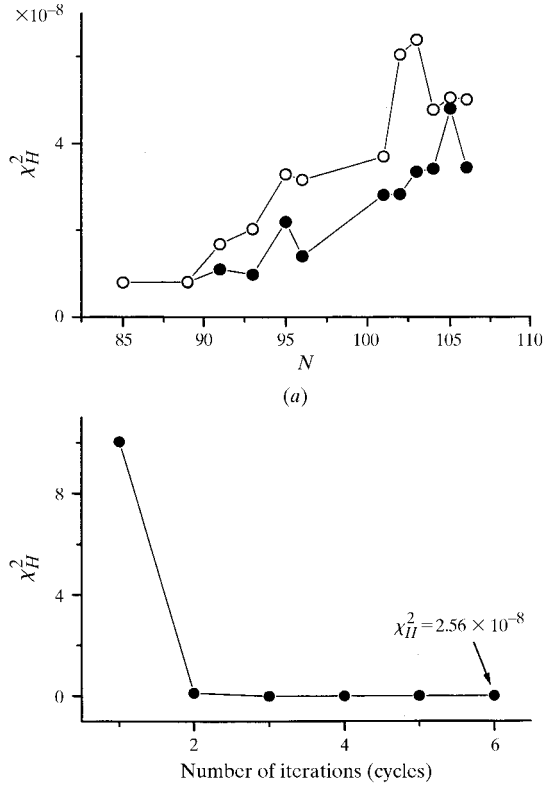

Figure 5
(*a*) χ^2_H *versus* N for correct phases (solid circles) and wrong phases (open circles). (*b*) Convergence of χ^2_H *versus* the number of iterations.

(iv) From phase extension for a few reflections at low resolution, it is sometimes difficult to get correct values. We speculate that it might be due to lacking connections to other reflections in multibeam interactions. Increasing the number of pixels may sometimes help because the larger the number of reflections involved in the entropy maximization, the more connections among the reflections can be established.

In conclusion, we have demonstrated that, using the phases determined from multibeam experiments as input to the maximum-entropy calculation scheme derived in this paper, we are able to generate more than 100 known phases without carrying out further experiments. Refinement of the experimental phases can also be achieved. Approximate electron-density maps can be calculated. The applicability of this phase-determination scheme is not limited to small crystals. Macromolecular crystals can be handled by increasing the number of pixels in the calculation. Up to now, with the help of a supercomputer, a $64 \times 64 \times 64$ pixels calculation can be executed with our program. The present approach may provide an alternative way for phase determination and extension.

The authors are indebted to the National Science Council for financial support and CMW and CHC are very grateful to the same organization for providing a postdoctoral and a graduate fellowship respectively during the course of this study. Assistance in verifying the structure using direct methods from Dr K. Rees and Professor H. Schenk is also gratefully acknowledged.

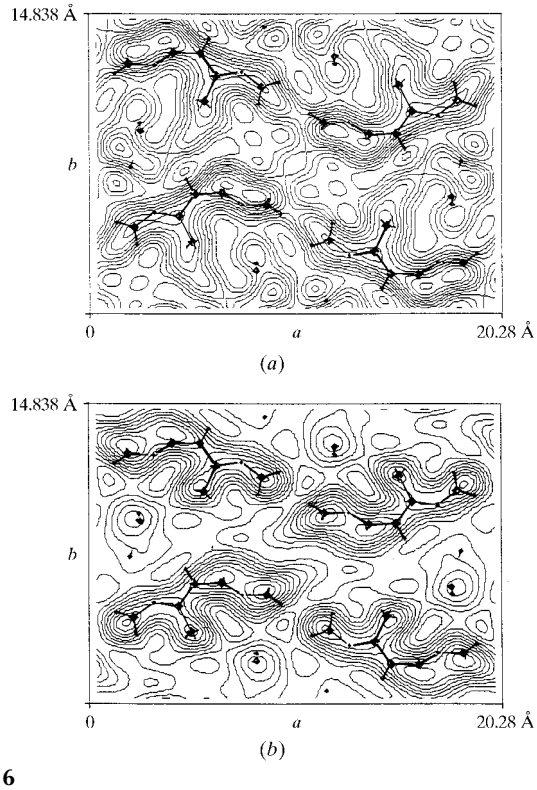

Figure 6
The electron-density maps of the *ab* plane: (*a*) calculated from entropy maximization; (*b*) calculated from the known structure. The fragments of benzene rings are shown as a guide to the eye. The contour interval is 0.002 e $Å^{-3}$.

References

Bricogne, G. (1984). *Acta Cryst.* A**40**, 410–451.
Bricogne, G. & Gilmore, C. J. (1990). *Acta Cryst.* A**46**, 284–297.
Chang, C. J., Fang, J. M., Lee, G. H. & Wang, Y. (1994). *J. Chem. Soc. Perkin Trans. 1*, pp. 3587–3593.
Chang, S. L. (1982). *Phys. Rev. Lett.* **48**, 163–166.
Chang, S. L. (1984). *Multiple Diffraction of X-rays in Crystals.* Berlin: Springer-Verlag.
Chang, S. L. (1998). *Acta Cryst.* A**54**, 886–894.
Chang, S. L., Chao, C. H., Huang, Y. S., Jean, Y. C., Sheu, H. S., Liang, F. J., Chien, H. C., Chen, C. K. & Yuan, H. S. (1999). *Acta Cryst.* A**55**, 933–938.
Chang, S. L., King, H. E. Jr, Huang, M. T. & Gao, Y. (1991). *Phys. Rev. Lett.* **67**, 3113–3116.
Chang, S. L., Stetsko, Y. P., Huang, Y. S., Chao, C. H., Liang, F. J. & Chen, C. K. (1999). *Phys. Lett. A*, **264**, 328–333.
Chang, S. L. & Tang, M. T. (1988). *Acta Cryst.* A**44**, 1065–1072.
Chang, S. L. & Wang, C. M. (1996). *Acta Cryst.* A**52**, C52.
Chapman, L. D., Yoder, D. R. & Colella, R. (1981). *Phys Rev. Lett.* **46**, 1578–1581.
Drabold, D. A. & Sankey, O. F. (1993). *Phys. Rev. Lett.* **70**, 3631–3634.
Han, F. S. & Chang, S. L. (1983). *Acta Cryst.* A**39**, 98–101.
Høier, R. & Marthinsen, K. (1983). *Acta Cryst.* A**39**, 854–860.
Hölzer, K., Weckert, E. & Schroer, K. (2000). *Acta Cryst.* D**56**, 322–327.
Huang, M. T., Wang, C. M. & Chang, S. L. (1994). *Acta Cryst.* A**50**, 342–344.
Hümmer, K. & Billy, B. (1982). *Acta Cryst.* A**38**, 841–848.
Hümmer, K., Bondza, H. & Weckert, E. (1991). *Z. Kristallogr.* **195**, 169–188.
Hümmer, K., Schwegle, W. & Weckert, E. (1991). *Acta Cryst.* A**47**, 60–62.
Hümmer, K., Weckert, E. & Bondza, H. (1989). *Acta Cryst.* A**45**, 182–187.
Hümmer, K., Weckert, E. & Bondza, H. (1990). *Acta Cryst.* A**46**, 393–402.
Juretschke, H. J. (1982). *Phys Rev. Lett.* **48**, 1487–1489.
Mo, F., Hauback, B. C. & Thorkildsen, G. (1988). *Acta Chem. Scand.* A**42**, 130–138.
Mo, F., Mathiesen, R. H., Alzari, P. M., Lescar, J. & Rasmussen, B. (1998). *Materials Structure in Chemistry, Biology, Physics and Technology*, Vol. 5, edited by R. Kuzel, J. Lhotha & L. Dobiasova, p. 484. Praha: Czech and Slovak Crystallographic Association.
Post, B. (1977). *Phys. Rev. Lett.* **39**, 760–763.
Press, W. H., Teukolsky, S. A., Vetterling, W. T. & Flannery, B. P. (1992). *Numerical Recipes in C.* Cambridge University Press.
Renninger, M. (1937). *Z. Kristallogr.* **97**, 107–121.
Rossmann, M. G. (1972). Editor. *The Molecular Replacement Method.* New York: Gordon and Breach.
Schenk, H. (1991). Editor. *Direct Methods for Solving Crystal Structures.* New York: Plenum Press.
Shen, Q. (1998). *Phys. Rev. Lett.* **80**, 3268–3271.
Shen, Q. & Colella, R. (1987). *Nature (London)*, **329**, 232–234.
Shen, Q. & Finkelstein, K. D. (1990). *Phys. Rev. Lett.* **65**, 3337–3340.
Shen, Q., Kycia, S. & Dobrianov, I. (2000). *Acta Cryst.* A**56**, 264–267.
Weckert, E., Hölzer, K., Schroer, K., Zellner, J. & Hümmer, K. (1999). *Acta Cryst.* D**55**, 1320–1328.
Weckert, E. & Hümmer, K. (1997). *Acta Cryst.* A**53**, 108–143.
Weckert, E., Schwegle, W. & Hümmer, K. (1993). *Proc. R. Soc. London Ser. A*, **442**, 33–46.
Woolfson, M. M. & Fan, H. F. (1995). *Physical and Non-Physical Methods of Solving Cystal Structures.* Cambridge University Press.